Pyroelectric energy harvesting for water splitting

Mengying Xie[a*], Steve Dunn[b], Emmanuel Le Boulbar[c] and Chris. R. Bowen[a*]

[a]Department of Mechanical Engineering, University of Bath, Claverton Down, Bath BA2 7AY, United Kingdom.

[b]School of Engineering and Materials Science, Queen Mary University of London, Mile End Road, London E1 4NS, United Kingdom.

[c]Department of Electronic and Electrical Engineering, University of Bath, Claverton Down, Bath BA2 7AY, United Kingdom.

[*]Corresponding author. Fax: +44(0)1225386928. Department of Mechanical Engineering, University of Bath, Claverton Down, Bath BA2 7AY, United Kingdom. Email addresses: M.Xie@bath.ac.uk, C.R.Bowen@bath.ac.uk

Highlights

1. First demonstration of water splitting using a pyroelectric energy harvesting system.
2. Materials and geometry selection to achieve critical electrical potential for electrolysis and maximise charge generation.
3. Use of rectification to generate hydrogen and oxygen at opposing electrodes during heating and cooling cycles.

Abstract

Hydrogen fuel cells are a promising energy conversion technology due to its high energy density and zero greenhouse gas emission. As a result, the production of hydrogen from renewable and alternative resources has gained significant interest in recent decades. This paper demonstrates a new approach which uses a pyroelectric energy harvester for water splitting and represents a novel alternative hydrogen source. Pyroelectrics are attractive for harvesting waste heat due to their ability to convert temperature fluctuations into electrical energy. A range of pyroelectric materials and geometries for water electrolysis are analysed to determine, (i) the minimum material thickness to generate a critical potential to initialise water decomposition and, (ii) to maximize the charge and hydrogen mass production. We then successfully demonstrate that an appropriate pyroelectric material, when combined with rectification of the alternating current, can harvest heat fluctuations and generate a sufficient electric potential difference and current for water splitting. By harvesting the pyroelectric electrical energy, a continuous hydrogen bubble production was observed during thermal cycling. Practical routes to maximize the level of hydrogen production for this new concept are also explored.

Keywords

Pyroelectric; Energy harvesting; Water splitting; Hydrogen

Introduction

1.1 Research Background

As evidence has shown that the emission of greenhouse gases, such as carbon dioxide, has been a significant contributor to global warming and climate change [1], renewable and alternative energy sources [2-6] have become one of the main topics of interest across the world. The fuel cell, particularly using hydrogen fuel, is one of the most promising energy conversion technologies [6, 7] due to its high energy density, low greenhouse gas emission and ease of storage. Today, the majority of hydrogen continues to be produced from fossil fuels and biomass [8, 9] and one problem of using fossil fuels and biomass is the difficulty of carbon dioxide capture and its confinement. As an alternative, hydrogen evolution from clean and renewable resources has gained significant interest over recent decades. One approach is to use photo-catalytic water splitting using a wide band semiconductor or a series of semiconductor heterojunctions [10-12] which can directly absorb sunlight and use the photo-excited carriers to electrochemically reduce and oxidize water simultaneously. In this case, titanium

dioxide (TiO_2) has been one of the most popular and widely used semiconductor in photo-catalyst research since the 1970s [13] and studies have focused on doping, surface decoration, core-shell structures and sacrificial reagents [12]. However, the number of available materials is limited and there remain concerns over performance and lifetime.

Recently, it has been reported that the piezoelectric effect can be coupled with electrochemical processes [14-17] and allows the engineering of charge-carrier conduction characteristics at the heterojunction between a strained piezoelectric material and a chemical solution. Hong and co-workers presented a "piezo-electro-chemical" effect where mechanical energy could be converted to hydrogen and oxygen [15]. In an ultrasonic water bath, the mechanical vibration of barium titanate and zinc oxide microfibers was reported to lead to the generation of strain-induced electric charges and the electric potential across the strained fibres was said to be sufficient to trigger the redox reaction and produce hydrogen and oxygen from water. Starr, *et al* [16] studied a "piezo-catalytic" effect for a single crystal cantilever of $Pb(Mg_{1/3}Nb_{2/3})O_3$-$32PbTiO_3$ coated with gold electrodes that was subjected to vibration in water. Their results showed that the rate of hydrogen production is dependent on the frequency of vibration and amplitude of the strain subjected to the cantilever, with hydrogen production increasing with increased piezoelectric potential, increased holding time and a decrease of electrolyte concentration. In addition to piezoelectric effects, "pyro-electro-catalysis", which combines the pyroelectric effect and an electrochemical oxidation-reduction reaction, has been studied and used for the disinfection of bacteria and decomposition of various toxic hazardous organic compounds in aqueous environments [18-20]. Gutmann, *et al.* and Benke, *et al*. focused on disinfection with nano- and micro-crystalline lithium niobate, lithium tantalite powder [18] and barium titanate/palladium nanoparticles [19]. When the powder was subjected to a temperature change, reactive oxygen species were created at the surface of the pyroelectric powders and react due to the uncompensated screening charge carriers. Later, Jiang, *et al.* [20] used bismuth ferrite nanoparticles to degrade a Rhodamine B dye solution using pyroelectric effects and it achieved a 99% degradation efficiency for a temperature change from 27°C to 38°C. Furthermore, water splitting using the pyroelectric effect has very recently been theoretically studied by Arvin, *et al.* using density functional theory [21]. In their model, the surface phase of lead titanate switches between the ferroelectric and paraelectric phase when subjected to cyclical temperature changes below and above the Curie temperature of the material respectively. In the lower temperature ferroelectric state, H_2O molecules are dissociated on the negatively poled surface to produce bound atomic hydrogen. When the material is switched to the higher temperature paraelectric phase, the hydrogen atoms recombine to form weakly bound H_2, thereby creating a clean surface that is ready for the next thermal cycle.

1.2 Pyroelectric Water Splitting

Heat, in particular low-grade waste heat, has been an attractive source of energy owing to its ubiquity in a variety of industrial applications as well as in the surrounding environment. Pyroelectric materials are of interest here since they have the potential to convert temperature fluctuations from waste heat into useful electrical energy. Pyroelectric materials are polar and exhibit a spontaneous polarization, P_s, in the absence of an applied electric field or mechanical displacement [22]. This spontaneous polarization leads to the presence of charge on each surface of the pyroelectric material and nearby free charges will be attracted to the surface as 'bound' charge. The origin of pyroelectric behaviour is understood from the behaviour of the surface charge as the ambient temperature is changed and assuming that the polarisation level is dependent on material temperature [22]. If the temperature of a pyroelectric is increased, the polarisation level decreases due to a reduction of the net dipole moment. The fall in the polarisation level then leads to a decrease in the number of charges bound to the material surface. If the material is under open circuit conditions the free charges remain at the electrode surface and an electric potential is generated across the material. If the material is under short circuit conditions an electric current flows between the two polar surfaces of the material. When the pyroelectric is subsequently cooled under short circuit conditions, the polarisation level is increased and leads to a reversal of the electric current flow under short circuit conditions.

In this study, we propose to use pyroelectric effect to generate a sufficiently large electric potential between two electrodes to split water into hydrogen and oxygen gas. Rather than position the pyroelectric material inside the electrolyte, we will place the material outside of the electrolyte to demonstrate the splitting of water assisted by pyroelectrics (SWAP). Electrolysis is the decomposition of water into hydrogen and oxygen and in order to trigger electrolysis and produce hydrogen gas, the overall potential difference between the anode and cathode is critical and, thermodynamically, the necessary potential difference is at least 1.23 V [23]. Eq. (1) and Eq. (2) provide the minimum electrode potential for electrolysis when *pH=0.* However, in reality an excess energy, termed an overpotential, is required to overcome activation energy barriers during the reaction. Additional factors are that some of the products may catalytically reconvert to water, oxygen might oxidise the anode, and a

double layer capacitor may be formed [16, 24, 25]. For example, in [25] water electrolysis requires at least 1.6 V when using nanoscaled TiO_2 and titanates.

$$\textit{Anode:} \qquad 2H_2O \rightarrow O_2 + 4H^+ + 4e^- \qquad E=\text{-}1.23V \qquad (1)$$

$$\textit{Cathode:} \qquad 2H^+ + 2e^- \rightarrow H_2 \qquad E=0.00V \qquad (2)$$

According to Faraday's laws of electrolysis, the mass of the substance produced by electrolysis is proportional to the quantity of carriers. This is expressed by Eq. (3), where m is the mass of the substance, Q is the total electric charge passed through the substance, F is the Faraday constant, M is the molar mass of the substance and z is the valence number of ions. Hence, in addition to the critical potential to initiate the reaction, the number of available charge carriers plays an important role in determining the amount of hydrogen that can be produced.

$$m = \frac{QM}{Fz} \qquad (3)$$

For pyroelectric materials, Eq. (4) defines the relationship between the rate of temperature change (dT/dt), generated charge (Q), pyroelectric current (I), surface area of the material (A), and pyroelectric coefficient (p) under short circuit conditions with electrodes that are orientated normal to the polar direction.

$$I = \frac{dQ}{dt} = pA\frac{dT}{dt} \qquad (4)$$

By integrating Eq. (4) with respect to time, the pyroelectric charge generated due to a temperature change (ΔT) is given by Eq. (5).

$$Q = pA\Delta T \qquad (5)$$

Since the pyroelectric material is typically a dielectric, the capacitance of the pyroelectric element as a parallel plate (e.g. as a thin film in Fig. 1a) is given by Eq. (6), where ε_{33}^T is the relative permittivity at constant stress, $\varepsilon_0$is permittivity of free space and h is the thickness of the material.

$$C = \frac{A\varepsilon_{33}^T\varepsilon_0}{h} \qquad (6)$$

Under open-circuit conditions, the pyroelectric charge (from Eq. (5)) leads to a potential difference across the material, given by $Q=CV$, which leads to Eq. (7),

$$V = \frac{p}{\varepsilon_{33}^T\varepsilon_0}h\Delta T \qquad (7)$$

Eq. (7) can therefore provide an indication of whether the potential difference generated by a pyroelectric element is sufficiently large to initiate electrolysis; e.g. 1.5V. The potential will depend on the thickness of the material, the temperature change and material properties (p/ε_{33}^T). In addition, Eq. (5) can provide an indication of the level of charge available for electrolysis, which is dependent on pyroelectric coefficient, surface area and temperature change. The two equations therefore indicate that a high p/ε_{33}^T, thickness and temperature change is necessary to generate the potential difference and in order to increase the generated electric charge and maximise the mass m of hydrogen it is necessary to select a material with high pyroelectric coefficient, large surface area, and subject it to a large temperature change.

1.3. Pyroelectric Material Selection

We now consider three common material configurations for the generation of the electric potential and charge; these are thin films/plates, particles and rods. These three configurations and an assumption of their polarisation direction can be seen in Fig. 1. If the material configuration is a rod (as in Fig. 1c), the h in the Eq. (1) and Eq. (2) is dependent on the direction of polarization. If the polarization is along to the rod growth direction, they can be considered as a discrete plate (as in Fig. 1a). Therefore, Fig. 1c shows the polarization perpendicular to the rods growth direction. Eight different pyroelectric materials are examined here that contain ferroelectric and non-ferroelectric materials along with single crystals, polycrystalline ceramics and a polymer. The material properties of relevance, i.e. pyroelectric coefficient, permittivity, density and Curie temperature, can be found in Table 1. The pyroelectric coefficient and permittivity are of importance as they relate to the voltage and charge, the density relates to the amount of material per unit mass and the Curie temperature defines the upper working temperature of the polarized material.

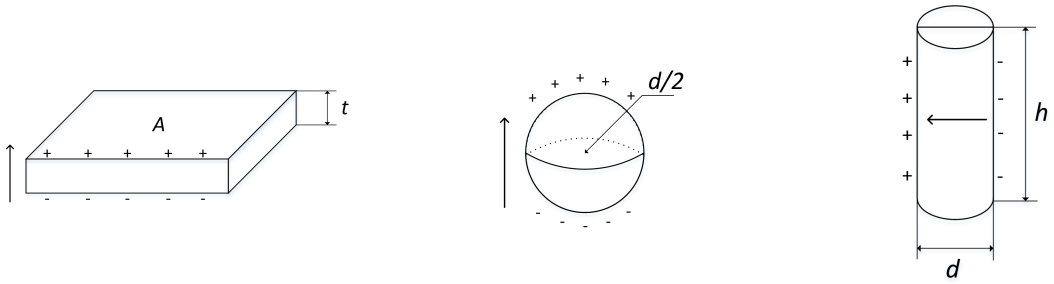

(a) (b) (c)

Fig. 1. Pyroelectric materials in the form of (a) flat thin film, (b) particles and (c) rods. The polarization direction of the material is indicated with an arrow in each configuration.

Table 1. Pyroelectric coefficient, relative permittivity, density and Curie temperature of a range of pyroelectric materials.

Material	p **(μC m^{-2}K^{-1})**	ε_{33}^{T}	**Density (g/cm^3)**	**Curie temperature (°C)**	**Reference**
Zinc oxide (ZnO)	-9.4	11	5.60	127	[26], [27], [28]
Lithium niobate ($LiNbO_3$)	-83	28.7	4.65	1210	[26], [29]
Lithium tantalite ($LiTaO_3$)	-230	47	7.45	665	[30]
Polyvinylidene fluoride (PVDF)	-27	12	1.78	80	[31]
Lead zirconate titanate (PZT-5H)	-380	3200	7.60	350	[26], [32], [33]
Barium titanate ($BaTiO_3$)	-200	1200	6.02	120	[26], [34]
Triglycine sulphide (TGS)	-280	38	1.69	49	[35]
Lead magnesium niobate lead titanate (PMN-0.25PT)	-746	2100	8.20	121	[36]

For the thin film configurations, the relationship between the developed voltage and film thickness along the polarisation direction can be readily calculated according to Eq. (7). In this case, we examine a voltage-thickness relationship for the range of materials assuming a constant temperature change of the pyroelectric material (1°C); the data is presented in Fig. 2. In addition, it is assumed that hydrogen evolution requires an overpotential of 0.27V [37], so that the necessary total potential is 1.5V for electrolysis. This target of 1.5V is also shown in Fig. 2 to indicate the minimum thickness needed for each pyroelectric film for a 1°C temperature change. It can be seen that many of the materials generate a sufficiently large potential despite the small temperature fluctuation; most materials require a thickness of less than 10μm to generate 1.5V for a 1°C temperature change. It is of interest to note that the materials than achieve the required voltage for a thickness of less than 10μm are all materials with low permittivity (see Fig. 2 and Table 1). Clearly, applying a temperature change that is higher than 1°C can enable even thinner films to generate a sufficient potential difference. For the particle and rod configuration, the voltage trends are the same as the thin film in Fig. 2 but the required electrolysis potential needed is likely to be higher as the distance between the positive and negative charge centres changes along the surface. For example, one assumption for such configurations can be that to generate the same potential difference as a thin film (Fig. 1a), the particle in Fig. 1b should be twice the diameter, since the centre of half sphere is $R/2$ to the thin film thickness and for a cylinder polarised normal to its length (Fig. 1c) the diameter needs to be 2.4 times as the centre of a half circle is $4\pi R/3$.

While Fig. 2 identifies materials, and their minimum thickness for a 1°C change, to make electrolysis thermodynamically favourable, Eq. (3) quantifies of amount of charge generated by the pyroelectric which will determine the mass of hydrogen produced. The electric charge a pyroelectric can generate for a temperature change of 1°C for the range of materials in Table 1 can be calculated by Eq. (7). Fig. 3a shows the relationship between the developed charge (Q) and the surface area (A) of pyroelectric materials in a thin film configuration (Fig. 1a).

For a particulate system, if it is assumed that half of the particle has a positive charge and another half is negative, as in Fig. 1b. Thus the surface area and pyroelectric charge developed with a temperature change of 1°C from 1 gram of material can be plotted in Fig. 3b. If it were rods with a polarisation direction as shown in Fig. 1c, the charges generated from 1 gram material would be 1/3 times to the particles ($Q_{rods} \propto 2/\rho d$, $Q_{particles} \propto 6/\rho d$, where ρ is the density of the material and d is the diameter).

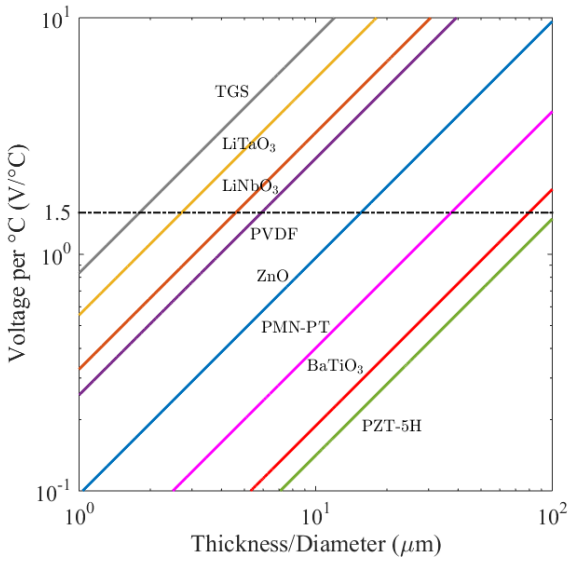

Fig. 2. Open circuit voltage generated for 1°C change vs. film thickness. Critical potential for electrolysis is indicated as 1.5V.

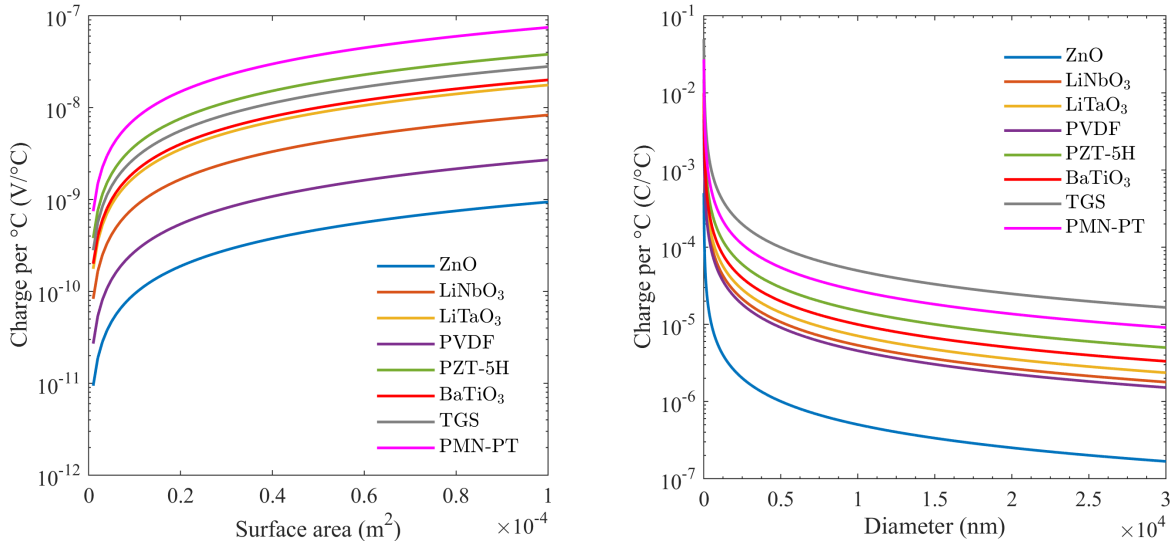

(a) (b)

Fig. 3. Charge generated for a 1°C temperature change for a range of pyroelectric materials. (a) Charge for thin films with a range of surface areas. (b) Charge for 1 gram of particles at a range of particle diameters.

By comparing the critical voltage (Fig. 2) and generated electric charge (Fig. 3) for a temperature change of 1°C for the range of materials in Table 1, it can be concluded that:

i) for all three configurations, the developed voltage is determined by the permittivity and pyroelectric coefficient of the materials; i.e. the p/ε_{33}^{T} ratio. The three materials that be able to generate the critical potential difference for the thinnest dimensions are TGS>$LiTaO_3$>$LiNbO_3$. The poorest materials are the ferroelectric ceramics PMN-PT, $BaTiO_3$, PZT-5H and this is due to their relatively high permittivity.

ii) for the **thin film** configurations, as in Fig. 1a, the developed charge is proportional to surface area and pyroelectric coefficient. For the same surface area, the best three materials are PMN-PT>PZT-5H>TGS. The poorest materials are PVDF and ZnO due to their low pyroelectric activity.

iii) for the **particle or rod** configuration (Fig. 1b and 1c respectively), the amount of generated charges depends on the material density, diameter of particles/rods, and pyroelectric coefficient. The best three materials are TGS>PMN-PT>PZT-5H. The poorest is ZnO due to its low piezoelectric activity and relatively high density.

Although PMN-PT has the highest pyroelectric coefficient and generates the largest amount of charge in thin film form (Fig. 3a), the high relative permittivity of this material makes it difficult to generate sufficient voltage for water electrolysis with thin or small structures (see Fig. 2); it should also be noted that while the relative permittivity is 2100 in Table 1, even higher values are reported for single crystal materials [36]. Triglycine sulphide (TGS) is able produce a sufficient potential at a small thickness or diameter (Fig. 2) and it pyroelectric activity has the capability to generate high levels of charge (Fig. 3a). However, the low curie temperature of TGS (49°C) limits its applications that operate above room or ambient temperatures and it is also soluble in water [38]. Lead zirconate titanate (PZT) has a high Curie temperature of 350°C [33] compared to PMN-PT (121°C [36]) and TGS (49°C [35]) and makes it possible to be used in high temperature applications. Low permittivites have been reported for PZT materials, such as 290 [35]. Although the ability for charge generation of PVDF film is not large, due to its low pyroelectric coefficient, see Fig. 3a, the flexibility, compatibility and ease of fabrication make it popular in many energy harvesting research and applications [39]. The high p/ε_{33}^{T} of PVDF also enables the required potential to be attained for small thickness films (Fig. 2). For these reasons we have selected PZT-5H thin films (>100µm, from Fig. 2) to demonstrate the pyroelectric energy harvesting system for water splitting and compared the effect with a flexible PVDF film (>5µm, from Fig. 2).

Experimental details

Fig. 4 shows the experimental setup for pyroelectric water splitting. The pyroelectric materials used in this study were lead zirconate titanate (PZT-5H) thin film (thickness of 127µm) and polyvinylidene fluoride (PVDF) thin film (thickness of 52µm). The surface area of both the PZT and PVDF thin films were 70 × 70 mm^2. A heat lamp (Philips type IR175W, diameter 121mm) was used to simulate the heat source. Temperature oscillations were realised by switching the lamp periodically on and off using a variable frequency controller covering the switching frequency range from mHz to Hz. Due to the small ratio of thickness to surface area of the pyroelectric layer, the natural convection with air was the main cooling system. The lamp heating-cooling cycle frequency in this study was 0.1Hz. The pyroelectric materials were placed at a 15cm distance from the heat lamp. The surface temperature of the pyroelectric material was measured using a K-type thermocouple and the thermocouple response time was 0.5s. A solution of 1M KOH was used as the electrolyte and two platinum microelectrodes were used as electrodes. The open circuit voltage or charge produced and closed circuit current were measured using Keithley 6517B electrometer with high input impedance (>200TΩ) for voltage measurements and <1fA noise. The power of the heat lamp was characterized with a calibrated thermal power sensor (THORlabs) at 15cm distance to the lamp and Fig. 5 shows the thermal power that is available for absorption.

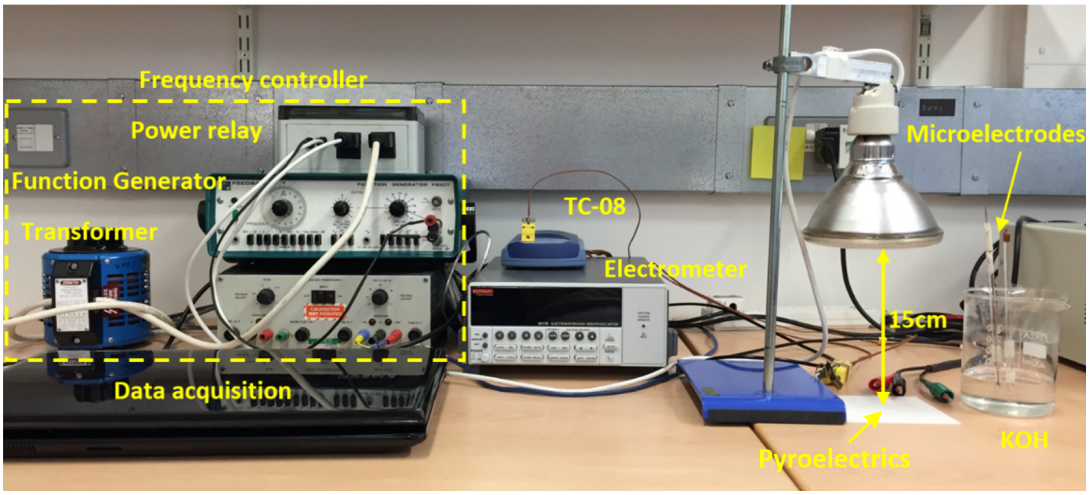

Fig. 4. Experimental setup for splitting of water using pyroelectrics.

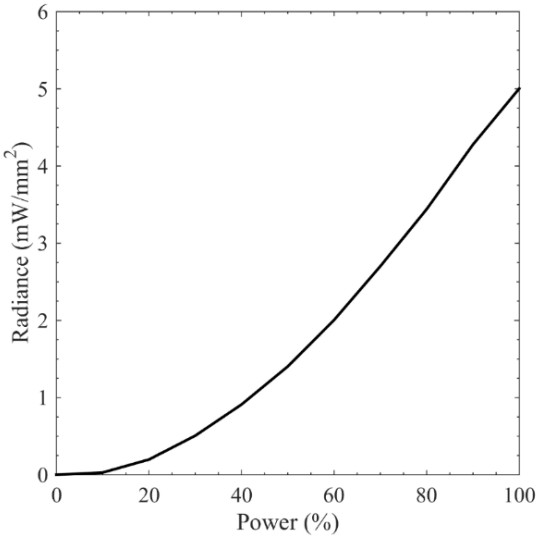

Fig. 5. Lamp irradiance intensity with increasing electrical power.

Results and discussion

Fig. 6 shows the measured surface temperature of the PZT and PVDF thin films and the measured open-circuit voltage during the temperature oscillations. The measured relative permittivity of PZT and PVDF are approximately 3800 and 11.5 , respectively as determined using a Solartron 1260 and 1296 Dielectric Interface. Using Eq. (5), (6), and (7) the charge generated by both the PZT and PVDF thin films can be calculated and are also shown in Fig. 6. The average temperature change of PZT and PVDF are similar but the peak-to-peak voltages are approximately 5V to 15V respectively; the higher voltage of the PVDF is due to the higher p/ε_{33}^{T} of the material that leads to a high open circuit voltage, despite the thickness being smaller (see Eq. (7)). The peak-to-peak predicted charge levels are different by an order of magnitude and this is simply due to the higher pyroelectric coefficient of the PZT; see Table 1 and Fig. 3a. Fig. 6b and 6d present the measured surface temperature of PZT and PVDF thin films measured under closed-circuit conditions. The rate of temperature change was calculated was for time-temperatude data and the shapes of the close circuit current agrees well with the rate of temperature change of both pyroelectric material (Eq. (4)). By fitting the closed circuit current and the rate of temperature change with the aid of Eq. (4), the pyroelectric coefficient can be estimated and are shown in Table 2. The estimated values (PVDF:22μCm^{-2}K^{-1}, PZT:280μCm^{-2}K^{-1}) have some difference from the pyroelectric coefficient presented in Table 1 extracted from the literature (PVDF:27μCm^{-2}K^{-1}, PZT:380μCm^{-2}K^{-1}). Differences may relate to the temperuature measurement relating to the surface temperature, conductivity losses and different material properties.

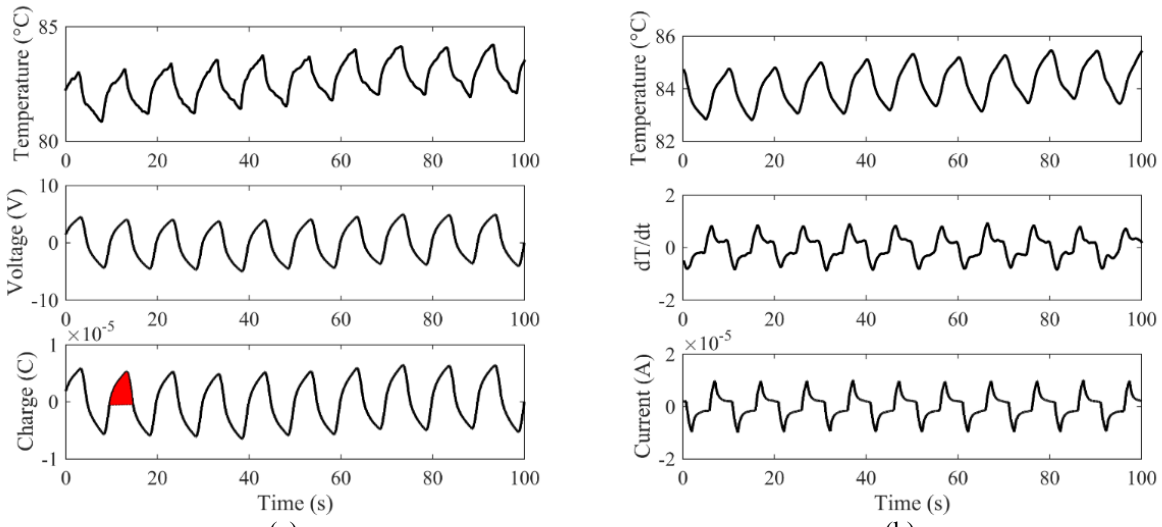

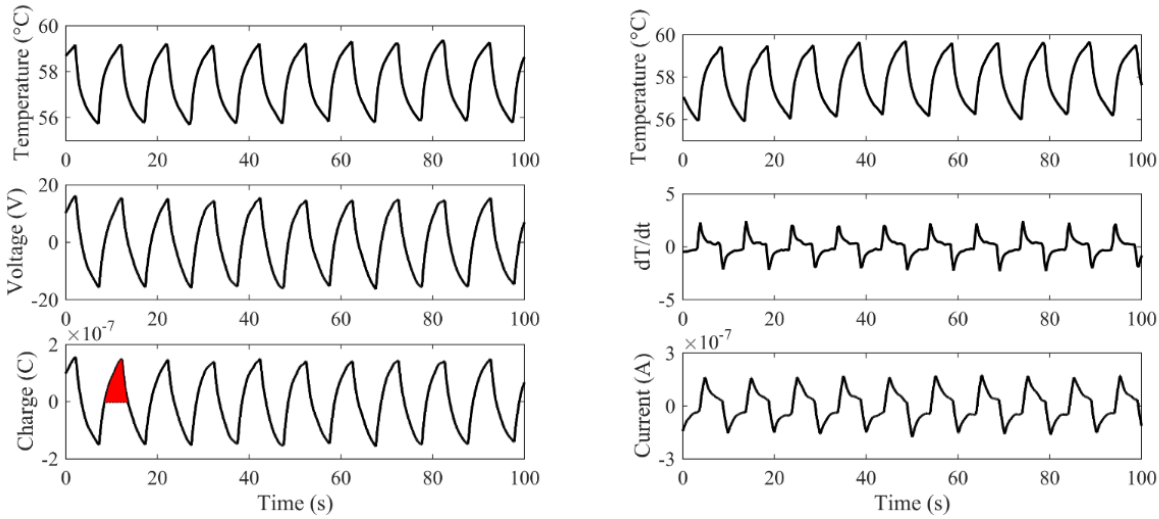

Fig. 6. Pyroelectric energy harvesting results for PZT-5H and PVDF thin films. (a-b) the surface temperature, open circuit voltage, generated charge, rate of temperature change, and measured current within PZT thin film; (c-d) the surface temperature, open circuit voltage, generated charge, rate of temperature change, and measured current within PVDF thin film.

From the experimental data, it is possible to predict the volume of hydrogen that can be generated on one of platinum microelectrodes during a half heating-cooling cycle. The accumulated charges developed in a half cycle on one electrode, which are highlighted as red in Fig. 6a and 6c; this can be calculated simply by integrating the charges with time in a half cycle and the values are shown in Table 2. PZT can generate 3.2×10^{-4}C charge, which is around two orders magnitude more than PVDF. Using Faraday's laws (Eq. (3)) and ideal gas law, $PV=nRT$, the ideal volume of hydrogen generated in half cycle from PVDF and PZT are 1.05nL and 40.9nL, respectively.

Table 2. Comparison of properties between the PVDF and PZT-5H thin films used in this study.

Material	**PVDF**	**PZT-5H**
Pyroelectric coefficient ($\mu Cm^{-2}K^{-1}$)	22	280
Relative permittivity	11.54	3800
Thickness (μm)	52	127
Surface area (m^2)	49×10^{-4}	49×10^{-4}
Calculated charges generated in half cycle (C)	8.1351×10^{-6}	3.1762×10^{-4}
Volume of hydrogen generated in half cycle (nL)	1.05	40.9

As the natural temperature oscillations lead to an increase and decrease of polarisation of the pyroelectric energy harvester it will generate alternative positive and negative voltage and current, as in Fig. 6, and in one heating-cooling cycle both hydrogen and oxygen gas are formed at each electrode during half cycles. This may cause problems [40] such as hydrogen and oxygen recombination [41] during the reaction which subsequently decreases the efficiency of electrolysis or simply makes collection of any generated oxygen and hydrogen problematic. This can be solved by connecting the pyroelectric energy harvester to a full wave bridge rectifier circuit to maintain the polarity of the AC current generated by the harvester, and the electrodes in Fig. 4. The rectifier circuit used was formed from four Vishay GP02 diodes, which is shown in Fig. 7. Fig. 8 shows the generated voltage and charge from the PVDF and PZT thin films with the rectifier circuit. It can be noticed that the amplitude of the generated voltage is smaller than the measurement without rectifier circuit and this is a result of the forwarding voltage of the diodes. With rectification, the hydrogen and oxygen can be only generated on one electrode in one heating-cooling cycle and similar to the non-rectifier situation, the created charge in a single cycle can be calculated. Therefore, the charge generated after rectification are 1.5×10^{-5} C and 5.1×10^{-4} C for PVDF and PZT thin film respectively and the volume of hydrogen gas generated in one cycle are

1.89nL and 66nL (compared to an estimated 2.10nL and 81.8nL without rectification). More efficient rectification circuits are available, for example the voltage drop can be smaller if it is replaced with a more efficient rectifier circuit such as PEHPS-PCB3 [42]. Nevertheless, it is clear that rectification can help maintain hydrogen and oxygen production at electrode.

Finally, this pyroelectric water splitting was tested with experimental setup as shown in Fig. 4. The 127μm thick PZT-5H thin film and rectifier circuit were used and PZT was chosen because of the larger charge generation capability compared to PVDF. When the measured charge generated in a half cycle was approximately 1.4×10^{-4}C, continuous hydrogen bubbles were observed, where a bubble could be seen to be generated in each half cycle; this can be found in the associated video.

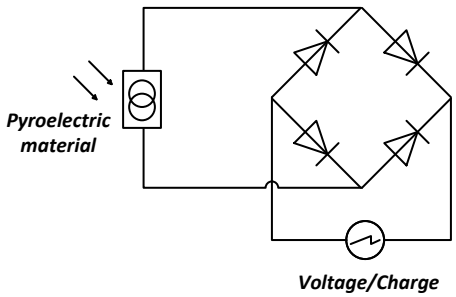

Fig. 7. Rectifier circuit employed to pyroelectric energy harvester to generate hydrogen and oxygen at each electrode.

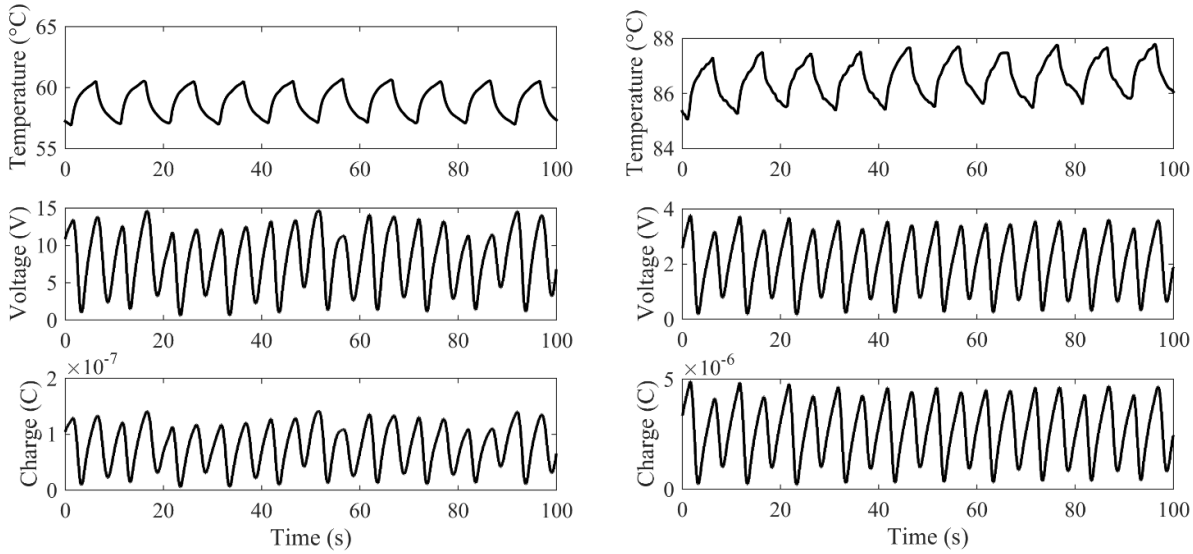

Fig. 8. Generated voltage and charge from PZT-5H and PVDF thin films after rectification.

Conclusion

This paper presents the first practical demonstration of novel a pyroelectric energy harvester for water splitting applications. Potential pyroelectric materials and geometries for water electrolysis using three material configurations in the form of thin film, particles and rods, have been analysed for polymeric, single crystal, and polycrystalline ceramic materials that include ferroelectric and non-ferroelectric systems. For a given temperature change, the minimum material thickness to generate a critical potential that initialises water decomposition for a range of materials were compared and are dependent on the materials properties, p/ε_{33}^{T} and temperature change. The charge developed is related to the pyroelectric coefficient and the area of the thin film material surface area and particle/rods diameter, which are also discussed and analysed. These comparisons provide a route for the selection of pyroelectric materials for the purpose of harvesting charges and tailoring the

geometry to develop sufficient potential for electrolysis and maximise the charge to generate hydrogen. The analysis shows that pyroelectric materials can readily generate a sufficiently high potential, but a relatively low current, and charge, when subjected to a change in temperature.

Most importantly, we have demonstrated that a pyroelectric energy harvesting system is able to split water and generate hydrogen gas simply using a pyroelectric element, such as PZT, in thin film form. Open circuit voltage, close circuit current and generated charges have been studied and a full wave bridge rectification circuit was used to ensure hydrogen was generated at only one electrode. Hydrogen gas bubbles were observed during each half cycle when the potential was created by PZT-5H polycrystalline ceramic thin film subjected to a small cyclic temperature change (2-4°C).

There are a variety of potential routes in order to increase hydrogen production, for example the PZT thin film could be simply replaced by PMN-PT, which has higher pyroelectric coefficient and generate larger charge levels. An additional approach would be to maximize the area of the pyroelectric either by simply using larger materials or creating highly nanostructured or porous surfaces, or using materials in particulate form. Very large polarization changes are also exhibited near the Curie-temperature; for example the magnitude of the pyroelectric coefficient increase significantly as the material approaches its Curie temperature since the level of polarization falls greatly with temperature in this region. Such routes are of interest to explore the splitting of water assisted using pyroelectrics reported here.

Acknowledgement

This work was supported by grant from the European Research Council (No. 320963) on Novel Energy Materials, Engineering Science and Integrated Systems (NEMESIS).

References

[1] Kyoto Protocol to the United Nations Framework Convention on Climate Change. http://unfccc.int/essential_background/kyoto_protocol/items/1678.php; [accessed 11.10.16].
[2] Harris P, Skinner W, Bowen CR, Kim HA. Manufacture and Characterisation of Piezoelectric Broadband Energy Harvesters Based on Asymmetric Bistable Cantilever Laminates. Ferroelectrics. 2015;480:65-76.
[3] Zabek D, Taylor J, Boulbar EL, Bowen CR. Micropatterning of flexible and free standing polyvinylidene difluoride (PVDF) films for enhanced pyroelectric energy transformation. Advanced Energy Materials. 2015;5.
[4] Turkenburg WC, Beurskens J, Faaij A, Fraenkel P, Fridleifsson I, Lysen E, et al. Renewable energy technologies. World Energy Assessment: Energy and the challenge of sustainability. 2000:219-72.
[5] Turner JA. A realizable renewable energy future. Science. 1999;285:687-9.
[6] Lucia U. Overview on fuel cells. Renewable and Sustainable Energy Reviews. 2014;30:164-9.
[7] Chan CC. The state of the art of electric, hybrid, and fuel cell vehicles. Proceedings of the IEEE. 2007;95:704-18.
[8] Chiarello GL, Aguirre MH, Selli E. Hydrogen production by photocatalytic steam reforming of methanol on noble metal-modified TiO2. Journal of Catalysis. 2010;273:182-90.
[9] Navarro R, Pena M, Fierro J. Hydrogen production reactions from carbon feedstocks: fossil fuels and biomass. Chemical reviews. 2007;107:3952-91.
[10] Walter MG, Warren EL, McKone JR, Boettcher SW, Mi Q, Santori EA, et al. Solar Water Splitting Cells. Chemical Reviews. 2010;110:6446-73.
[11] Chen X, Shen S, Guo L, Mao SS. Semiconductor-based photocatalytic hydrogen generation. Chemical reviews. 2010;110:6503-70.
[12] Kudo A, Miseki Y. Heterogeneous photocatalyst materials for water splitting. Chemical Society Reviews. 2009;38:253-78.
[13] Fujishima A. Electrochemical photolysis of water at a semiconductor electrode. nature. 1972;238:37-8.
[14] Starr MB, Wang X. Coupling of piezoelectric effect with electrochemical processes. Nano Energy. 2015;14:296-311.
[15] Hong K-S, Xu H, Konishi H, Li X. Direct Water Splitting Through Vibrating Piezoelectric Microfibers in Water. The Journal of Physical Chemistry Letters. 2010;1:997-1002.
[16] Starr MB, Shi J, Wang X. Piezopotential-Driven Redox Reactions at the Surface of Piezoelectric Materials. Angewandte Chemie International Edition. 2012;51:5962-6.
[17] Hong K-S, Xu H, Konishi H, Li X. Piezoelectrochemical effect: A new mechanism for azo dye decolorization in aqueous solution through vibrating piezoelectric microfibers. The Journal of Physical Chemistry C. 2012;116:13045-51.

[18] Gutmann E, Benke A, Gerth K, Böttcher H, Mehner E, Klein C, et al. Pyroelectrocatalytic disinfection using the pyroelectric effect of nano-and microcrystalline LiNbO3 and LiTaO3 particles. The Journal of Physical Chemistry C. 2012;116:5383-93.
[19] Benke A, Mehner E, Rosenkranz M, Dmitrieva E, Leisegang T, Stöcker H, et al. Pyroelectrically Driven •OH Generation by Barium Titanate and Palladium Nanoparticles. The Journal of Physical Chemistry C. 2015;119:18278-86.
[20] Wu J, Mao W, Wu Z, Xu X, You H, Xue AX, et al. Strong pyro-catalysis of pyroelectric BiFeO3 nanoparticles under a room-temperature cold-hot alternation. Nanoscale. 2016;8:7343-50.
[21] Kakekhani A, Ismail-Beigi S. Ferroelectric oxide surface chemistry: water splitting via pyroelectricity. Journal of Materials Chemistry A. 2016;4:5235-46.
[22] Bowen CR, Taylor J, LeBoulbar E, Zabek D, Chauhan A, Vaish R. Pyroelectric materials and devices for energy harvesting applications. Energy & Environmental Science. 2014;7:3836-56.
[23] Khan SUM, Al-Shahry M, Ingler WB. Efficient Photochemical Water Splitting by a Chemically Modified n-TiO2. Science. 2002;297:2243.
[24] Pletcher D. A first course in electrode processes: Royal Society of Chemistry; 2009.
[25] Osterloh FE. Inorganic nanostructures for photoelectrochemical and photocatalytic water splitting. Chemical Society Reviews. 2013;42:2294-320.
[26] Lang SB. Pyroelectricity: from ancient curiosity to modern imaging tool. Physics today. 2005;58:31.
[27] Young K, Frederikse H. Compilation of the static dielectric constant of inorganic solids. Journal of Physical and Chemical Reference Data. 1973;2:313-410.
[28] Jagadish C, Pearton SJ. Zinc oxide bulk, thin films and nanostructures: processing, properties, and applications: Elsevier; 2011.
[29] Weis R, Gaylord T. Lithium niobate: summary of physical properties and crystal structure. Applied Physics A. 1985;37:191-203.
[30] Lingam D, Parikh AR, Huang J, Jain A, Minary-Jolandan M. Nano/microscale pyroelectric energy harvesting: challenges and opportunities. International Journal of Smart and Nano Materials. 2013;4:229-45.
[31] Whatmore R. Pyroelectric devices and materials. Reports on progress in physics. 1986;49:1335.
[32] Gupta V, Sharma M, Thakur N, Singh S. Active vibration control of a smart plate using a piezoelectric sensor–actuator pair at elevated temperatures. smart materials and structures. 2011;20:105023.
[33] Vijaya M. Piezoelectric Materials and Devices: Applications in Engineering and Medical Sciences: CRC Press; 2012.
[34] Hayward G, Bennett J, Hamilton R. A theoretical study on the influence of some constituent material properties on the behavior of 1 - 3 connectivity composite transducers. The Journal of the Acoustical Society of America. 1995;98:2187-96.
[35] Gupta MC, Ballato J. The handbook of photonics: CRC press; 2006.
[36] Sebald G, Lefeuvre E, Guyomar D. Pyroelectric energy conversion: optimization principles. ieee transactions on ultrasonics, ferroelectrics, and frequency control. 2008;55:538-51.
[37] Rand DAJ, Dell R. Hydrogen energy: challenges and prospects: Royal Society of Chemistry; 2008.
[38] Renugadevi R, Kanchana G, Kesavasamy R. Growth and Characterization of Triglycine Sulphate (TGS) Single Crystals. 2013.
[39] Sodano HA, Inman DJ, Park G. A review of power harvesting from vibration using piezoelectric materials. Shock and Vibration Digest. 2004;36:197-206.
[40] Shipley JW. The alternating current electrolysis of water. Canadian Journal of Research. 1929;1:305-58.
[41] Wilber HW. Alternating Current Electrolysis with Zinc Electrodes in Sodium Thiosulphate Solution, [Master thesis]: Rice Institute; 1917.
[42] Non-linear AC-DC Converter for Piezoelectric Energy Harvesting Power Supplies. http://www.iis.fraunhofer.de/content/dam/iis/de/doc/lv/los/energie/2014_04_02_AC-DC%20Converter%20for%20Piezoelectric%20Power%20Supplies.pdf; 2014 [accessed 11.10.16].